Applied Physics Letters ARTICLE pubs.aip.org/aip/apl

An optical fiber integrated device for nonlinear generation of femtosecond mid-infrared pulses

Cite as: Appl. Phys. Lett. **124**, 261103 (2024); doi: 10.1063/5.0208093
Submitted: 13 March 2024 · Accepted: 16 June 2024 ·
Published Online: 27 June 2024

H. Kempf, M. Hagner, P. Sulzer, C. Riek, and A. Leitenstorfer[a)]

AFFILIATIONS

Department of Physics and Center for Applied Photonics, University of Konstanz, D-78457 Konstanz, Germany

[a)]Author to whom correspondence should be addressed: aleitens@uni-konstanz.de

ABSTRACT

Compact and broadband mid-infrared (MIR) sources are in high demand because of a wide range of potential applications such as molecular sensing in the fingerprint region. The generation of coherent MIR radiation at arbitrary frequencies typically requires nonlinear mixing between at least two input waves, which is often cumbersome to implement. We present an integrated and, therefore, adjustment-free solution combining few-femtosecond pulse compression in a germanosilicate optical fiber and optical rectification. To this end, a 16-μm-thin GaSe crystal is directly mounted on the end facet of a highly nonlinear fiber assembly exploiting a focused ion beam. With input pulses of a minute energy of 5 nJ and a duration of 120 fs at the telecom wavelength of 1.55 μm, we directly obtain ultrabroadband and phase-stable output transients. Electro-optic sampling in free space reveals single-cycle pulses with spectral components covering the entire MIR from 10 to 120 THz.

Coherent mid-infrared (MIR) light sources are powerful tools for a large number of tasks such as free-space telecommunication,[1,2] optical imaging,[3,4] precision spectroscopy in the molecular fingerprint region,[5–7] or subcycle quantum electrodynamics.[8] Broadband frequency combs can further enhance the performance of these applications by instantaneously covering a large part of the MIR spectrum and enabling the synthesis of short pulses. Nevertheless, a lack of broadband gain media in this region typically renders nonlinear frequency conversion inevitable. The leading methods for the generation of broadband MIR frequency combs are based on the downconversion of visible or near-infrared (NIR) laser sources through optical parametric oscillators[9–11] and amplifiers,[12–14] or optical rectification (OR) generating difference frequencies within a broadband optical pulse.[15–20] Parametric devices require precise alignment and stabilization of either the cavity or the two input beams. This aspect represents a challenge for compact turn-key solutions. In contrast, OR performs frequency conversion in a single beam, eliminating the need for temporal and spatial stabilization. This approach inherently provides carrier-envelope phase (CEP)-stable pulses as required for various applications like time-domain spectroscopy[21,22] or subcycle quantum electrodynamics.[8] Still, the generation of ultrashort and ultrabroadband MIR pulses with OR requires few-femtosecond pump pulses in the visible or NIR and precise focusing into a second-order nonlinear medium, which is prone to misalignment. In addition, field-resolved detection methods such as free-space electro-optic sampling (EOS) require exact imaging of the emitter region into the detection volume where they are overlapped with a subcycle probe. The nonlinear emitter crystal has to be transparent in the entire spectral range of the pump source and MIR output. With its high second-order nonlinearity and an infrared transmission window between 10 and 450 THz, GaSe represents an excellent option for this task.[15,23] Microstructuring and manipulation of this layered material may be achieved with a focused ion beam (FIB).[24]

Here, we demonstrate a compact device providing ultrabroadband MIR laser pulses directly from a fiber-based integrated component. Pump pulses with an energy of 5 nJ and a duration of 120 fs at the telecom wavelength of 1.55 μm are readily available from compact fs-Er:fiber laser technology. They are spectrally broadened and compressed below 20 fs in a highly nonlinear fiber (HNF) assembly. A GaSe crystal is placed directly on the end facet of this HNF, taking advantage of the small mode field diameter and circumventing any alignment requirements for OR. A commercial scanning electron microscope (SEM)-FIB system equipped with micromanipulators is harnessed to cut out and tailor the crystal, precisely transfer it to the end facet of the fiber and fix it in this position. The CEP-stable MIR output, as characterized with electro-optic sampling,[7,12,15,25,26] consists of single-cycle pulses spanning the entire MIR spectral region.

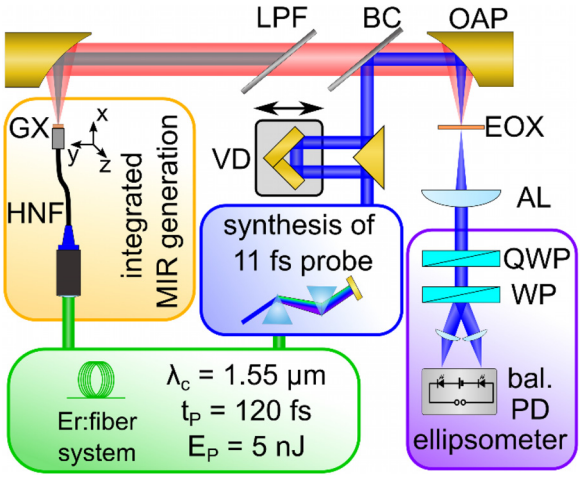

FIG. 1. Scheme of the experimental setup. A two-branch Er:fiber laser system provides 120 fs pulses with energies of 5 nJ at a repetition rate of 40 MHz (green frame). The first branch acts as input for the integrated component (orange frame) consisting of a highly nonlinear fiber (HNF) and the second-order nonlinear generation crystal (GX, 16 μm thick GaSe). OR results in an ultrabroadband MIR spectrum. To detect the output with EOS, an ultrashort probe with a pulse duration of 11 fs is synthesized in the second branch (blue frame). Both pulses are focused into a nonlinear electro-optic crystal (EOX, 10 μm of GaSe), and an ellipsometer (purple frame) reads out the induced polarization change on the probe. VD: variable optical delay stage; LPF: longpass filter (150 μm of GaSb); BC: beam combiner (500 μm of Si); OAP: off-axis parabolic mirror; AL: achromatic lens; QWP: quarter-wave plate; WP: Wollaston prism; bal. PD: balanced photodiodes.

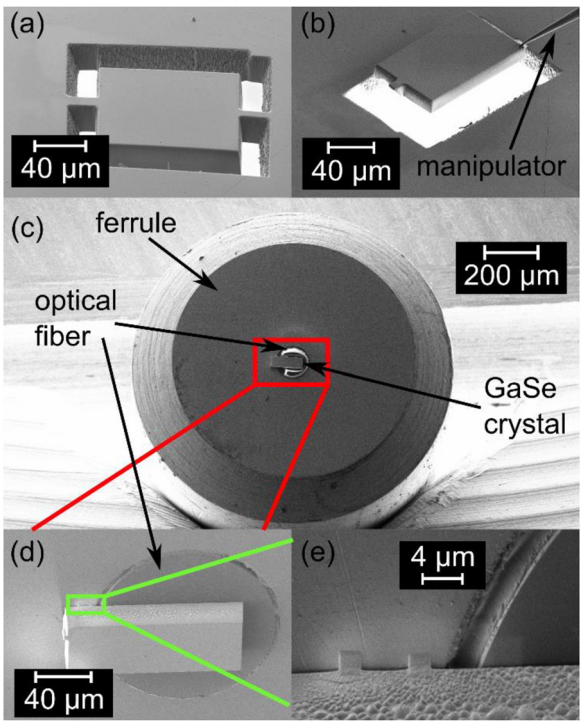

FIG. 2. SEM micrographs of the fabrication steps of the integrated element. (a) Microscopic emitter crystal precut into a GaSe sample of 16 μm thickness with a Ga^+ focused ion beam (FIB). (b) A sharp tungsten tip (black arrow) is attached to the precut crystal with gas-assisted deposition of platinum, enabling transfer to the fiber after removing the support bridges with FIB. (c) Front view of the optical fiber with metallic ferrule and mounted GaSe crystal. (d) Close up view of the red frame in (c), showing the emitter crystal covering the core region of the HNF and overlapping the ferrule. (e) Close up of the green frame in (d), featuring the contacts fabricated by gas-assisted Pt deposition to achieve adequate thermal contact and mechanical stability.

The experimental setup for implementation and characterization of the integrated element is depicted in Fig. 1. It is based on a mode-locked Er:fiber oscillator operating at a repetition rate of 40 MHz followed by two parallel femtosecond Er:fiber amplifiers (green panel). A fiber-coupled electro-optic modulator reduces the repetition rate of the first branch to 20 MHz, enabling a radio frequency lock-in scheme for shot-noise limited detection. The free-space output of this first branch serves as input for the ultrabroadband MIR generation in the integrated element (orange frame).

In a first step, the pump beam is efficiently guided into a polarization-maintaining standard telecom fiber (PM1550) with a commercial free-space coupling lens that is rigidly prealigned, rendering the setup immune to mechanical instabilities and acoustics. Inside the 10 cm of telecom fiber, the pulses experience solitonic compression down to durations on the order of several tens of femtoseconds. To this end, self-phase modulation spectrally broadens the pulse, while the anomalous dispersion of the fiber compensates for the accumulated phase, thus compressing the pulse in time.[27,28] The HNF is a germanosilicate fiber that is directly spliced to the PM1550 with negligible losses despite its smaller mode field diameter of 4 μm. Its length of 1 cm is selected to provide the shortest pulse possible without external dispersion control, resulting in a duration of 18 fs.[27,28]

The remaining pulse energy of 4 nJ serves as input for the second step: downconversion of the NIR spectrum to the MIR via OR in the GaSe nonlinear generation crystal (GX). This layered semiconductor supports exfoliation of very thin specimens directly from the bulk material.[29] In this way, we prepare a sample of 16 μm thickness and assemble a free-standing piece on a specially designed holder. Using a SEM-FIB system (Neon 40EsB from Carl Zeiss AG), a small piece of this GaSe sample is mounted directly on the end facet of the fiber.

To this end, both the HNF assembly and the GaSe sample are loaded into the SEM-FIB system. First, a small part (approximately 120 × 60 μm) of the crystal is precut with the focused Ga^+ ion beam at a current of 10 nA, while it is still connected to the sample on two opposite sides [see Fig. 2(a)]. In a second step, the micromanipulator (Kammrath and Weiss) positions a sharp tungsten tip on one corner of the precut crystal. Gas-assisted deposition of platinum, induced by the Ga^+ ion beam with a current of 10 pA, connects the tip to the crystal. Subsequently, the two support bridges to the main crystal are removed with the FIB at a current of 2 nA [Fig. 2(b)]. In a next step, the manipulator lifts out the crystal and precisely positions it onto the flat end facet of the HNF [Fig. 2(c)]. To enable complete monitoring with SEM, the HNF is attached to a 45° pre-tilted specimen holder. Furthermore, the optical fiber is terminated with a steel ferrule [Fig. 2(c)] offering three benefits: first, larger GaSe samples can be handled, increasing mechanical stability. Second, the metal serves as thermal sink that conducts excess heat introduced by the laser beam away

from the crystal. Third, it facilitates handling of the fiber in the optical setup. The first two aspects are further enhanced by connecting the GaSe crystal to the metallic ferrule with gas-assisted platinum deposition [Figs. 2(d) and 2(e)]. In this case, a beam current of 100 pA is exploited to increase the deposition rate and cover a larger area.

Mounting the nonlinear GX straight on the end facet of the HNF offers several advantages: (i) The small mode field diameter of the HNF of only 4 μm promises high peak fields, thus strong nonlinear effects inside the GX. (ii) Since the single-mode cutoff of the fiber is above the input wavelength, the transverse mode profile exiting the fiber is extremely close to a Gaussian, as desired for most applications. (iii) Any alignment of optical components for collimation of the fiber output and refocusing into the nonlinear crystal becomes obsolete. (iv) The end facet of the fiber device represents a diffraction-limited source of MIR radiation, which may be translated and rotated in all spatial dimensions without losing alignment.

To analyze the amplitude and phase of the electric field of the MIR output generated in the integrated element, we exploit the pulse train's inherent CEP stability and perform EOS (see Fig. 1). A 150-μm-thick GaSb filter removes the residual ultrashort pump centered around 1.55 μm, and the MIR electric field transient is spatio-temporally superposed with the probe using a variable optical delay followed by a Si wafer of 500 μm thickness. The probe pulse train at the full repetition rate of 40 MHz is synthesized by harnessing another custom-designed HNF to generate a broadband dispersive wave and subsequent temporal compression in a glass prism pair to a pulse duration of 11 fs (blue frame, Fig. 1).[27,28] This generation scheme enables precise dispersion control of the probe, ensuring maximally quantitative characterization of the MIR transient in amplitude and phase with EOS. An off-axis parabolic mirror focuses both beams into the electro-optic crystal (EOX, 10 μm of GaSe) in which the MIR electric field induces a polarization change of the probe via the Pockels effect. The probe is recollimated and passed onto the ellipsometer (purple frame, Fig. 1) consisting of a quarter-wave plate (QWP), Wollaston prism (WP), and balanced photodiodes (bal. PD). We demodulate the differential photocurrent at the repetition rate of the MIR pulses of 20 MHz with a radio frequency lock-in amplifier (UHFLI, Zurich Instruments). Operating at the first subharmonic of the probe pulse train provides optimum detection sensitivity by complete decoupling from any disturbances at, e.g., acoustic frequencies. The electric-field waveform of the MIR pulse is reconstructed by scanning the variable delay to the ultrashort probe.

The detected EOS transient is depicted in Fig. 3(a), disclosing a single-cycle MIR pulse with a duration of 23 fs. We expect an even shorter pulse duration close to the Fourier limit of 16 fs right after the integrated element. However, before its detection with EOS, the pulse becomes stretched in time due to the dispersion of the Si and GaSb wafers (BC and LPF in Fig. 1, respectively). The Fourier transform of the measured electric field transient unveils its spectral amplitude and phase [solid blue and dashed red lines, Fig. 3(b)]. The former exhibits a full-width at half-maximum of 32 THz at a center frequency of 46 THz (corresponding to a wavelength of 6.5 μm). In a logarithmic representation [Fig. 3(c)], the ultrabroadband character truly emerges with spectral components covering the entire MIR from 10 to 120 THz (corresponding to a wavelength range from 2.5 to 30 μm). In combination with an excellent signal-to-noise ratio of 125 in the spectral amplitude [Fig. 3(c), dashed line], thus 1.5×10^4 in intensity after a total

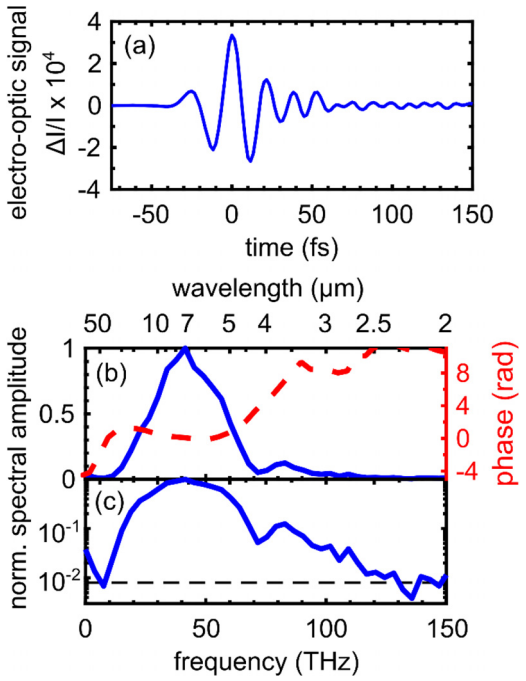

FIG. 3. Characterization of the MIR output of the integrated device by EOS. (a) Electro-optic signal vs optical delay time. (b) Normalized Fourier transform of (a) presenting the spectral amplitude (solid blue line) and phase (dashed red line). (c) Semilogarithmic plot of the normalized spectral amplitude with continuous coverage above the noise floor (dashed) between 10 and 120 THz.

measurement time of only 1 min, the device is ideally suited for spectroscopic applications in both frequency- and time-domain applications.[6,7,21]

In summary, we have presented a compact time-domain spectrometer based on Er:fiber technology covering almost the entire MIR. The key component is an integrated element combining synthesis of ultrashort pump pulses and the generation of ultrabroadband MIR radiation. It consists of a custom-designed HNF assembly and a nonlinear GaSe crystal that is tailored and mounted on the end facet by means of focused Ga^+ ions from a SEM-FIB system. Our device design offers the possibility of applying an additional antireflection coating[24] or cutting the crystal at a desired phase-matching angle. The inherently carrier-envelope phase-stable MIR output of the OR device was characterized with EOS: The single-cycle pulses are centered at a frequency of 46 THz (wavelength of 6.5 μm), covering the interval from 10 to 120 THz. The entire setup covers a footprint of less than 1 m^2 and offers easy alignment together with a high robustness despite the sub-cycle character of its approach.

This work was funded by the DFG—Project-ID 425217212—SFB 1432.

AUTHOR DECLARATIONS

Conflict of Interest

The authors have no conflicts to disclose.

Author Contributions

H. Kempf: Formal analysis (equal); Investigation (equal); Visualization (equal); Writing – original draft (equal); Writing – review & editing (equal). **M. Hagner:** Investigation (equal); Resources (equal); Writing – original draft (equal); Writing – review & editing (equal). **P. Sulzer:** Conceptualization (equal); Investigation (equal); Writing – review & editing (supporting). **C. Riek:** Conceptualization (equal); Writing – review & editing (supporting). **A. Leitenstorfer:** Conceptualization (equal); Funding acquisition (lead); Resources (equal); Supervision (lead); Writing – review & editing (lead).

DATA AVAILABILITY

The data that support the findings of this study are available from the corresponding author upon reasonable request.

REFERENCES

[1]K. Zou, K. Pang, H. Song, J. Fan, Z. Zhao, H. Song, R. Zhang, H. Zhou, A. Minoofar, C. Liu, X. Su, N. Hu, A. McClung, M. Torfeh, A. Arbabi, M. Tur, and A. E. Willner, "High-capacity free-space optical communications using wavelength- and mode-division-multiplexing in the mid-infrared region," Nat. Commun. **13**(1), 7662 (2022).

[2]H. Dely, T. Bonazzi, O. Spitz, E. Rodriguez, D. Gacemi, Y. Todorov, K. Pantzas, G. Beaudoin, I. Sagnes, L. Li, A. G. Davies, E. H. Linfield, F. Grillot, A. Vasanelli, and C. Sirtori, "10 Gbit s−1 free space data transmission at 9 μm wavelength with unipolar quantum optoelectronics," Laser Photonics Rev. **16**, 2100414 (2022).

[3]S. Türker-Kaya and C. Huck, "A review of mid-infrared and near-infrared imaging: Principles, concepts and applications in plant tissue analysis," Molecules **22**(1), 168 (2017).

[4]J. S. Dam, P. Tidemand-Lichtenberg, and C. Pedersen, "Room-temperature mid-infrared single-photon spectral imaging," Nat. Photonics **6**(11), 788–793 (2012).

[5]A. Schliesser, N. Picqué, and T. W. Hänsch, "Mid-infrared frequency combs," Nat. Photonics **6**(7), 440–449 (2012).

[6]A. V. Muraviev, V. O. Smolski, Z. E. Loparo, and K. L. Vodopyanov, "Massively parallel sensing of trace molecules and their isotopologues with broadband subharmonic mid-infrared frequency combs," Nat. Photonics **12**(4), 209–214 (2018).

[7]I. Pupeza, M. Huber, M. Trubetskov, W. Schweinberger, S. A. Hussain, C. Hofer, K. Fritsch, M. Poetzlberger, L. Vamos, E. Fill, T. Amotchkina, K. V. Kepesidis, A. Apolonski, N. Karpowicz, V. Pervak, O. Pronin, F. Fleischmann, A. Azzeer, M. Žigman, and F. Krausz, "Field-resolved infrared spectroscopy of biological systems," Nature **577**(7788), 52–59 (2020).

[8]C. Riek, P. Sulzer, M. Seeger, A. S. Moskalenko, G. Burkard, D. V. Seletskiy, and A. Leitenstorfer, "Subcycle quantum electrodynamics," Nature **541**(7637), 376–379 (2017).

[9]S. Chaitanya Kumar, A. Esteban-Martin, T. Ideguchi, M. Yan, S. Holzner, T. W. Hänsch, N. Picqué, and M. Ebrahim-Zadeh, "Few-cycle, broadband, mid-infrared optical parametric oscillator pumped by a 20-fs Ti: Sapphire laser," Laser Photonics Rev. **8**(5), L86–L91 (2014).

[10]A. Y. Hwang, H. S. Stokowski, T. Park, M. Jankowski, T. P. McKenna, C. Langrock, J. Mishra, V. Ansari, M. M. Fejer, and A. H. Safavi-Naeini, "Mid-infrared spectroscopy with a broadly tunable thin-film lithium niobate optical parametric oscillator," Optica **10**(11), 1535 (2023).

[11]H. Kempf, A. Muraviev, F. Breuning, P. G. Schunemann, R. Tenne, A. Leitenstorfer, and K. Vodopyanov, "Direct sampling of femtosecond electric-field waveforms from an optical parametric oscillator," APL Photonics **9**(3), 036111 (2024).

[12]A. Sell, A. Leitenstorfer, and R. Huber, "Phase-locked generation and field-resolved detection of widely tunable terahertz pulses with amplitudes exceeding 100 MV/cm," Opt. Lett. **33**(23), 2767 (2008).

[13]S. A. Rezvani and T. Fuji, "Millijoule 265 fs Tm:YAP regenerative amplifier for driving ultrabroad band collinear mid-infrared optical parametric amplifiers," Opt. Express **30**(5), 7332 (2022).

[14]G. Cerullo, A. Baltuška, O. D. Mücke, and C. Vozzi, "Few-optical-cycle light pulses with passive carrier-envelope phase stabilization," Laser Photonics Rev. **5**(3), 323–351 (2011).

[15]C. Kübler, R. Huber, S. Tübel, and A. Leitenstorfer, "Ultrabroadband detection of multi-terahertz field transients with GaSe electro-optic sensors: Approaching the near infrared," Appl. Phys. Lett. **85**(16), 3360–3362 (2004).

[16]P. Steinleitner, N. Nagl, M. Kowalczyk, J. Zhang, V. Pervak, C. Hofer, A. Hudzikowski, J. Sotor, A. Weigel, F. Krausz, and K. F. Mak, "Single-cycle infrared waveform control," Nat. Photonics **16**(7), 512–518 (2022).

[17]J. Zhang, K. Fai Mak, N. Nagl, M. Seidel, D. Bauer, D. Sutter, V. Pervak, F. Krausz, and O. Pronin, "Multi-mW, few-cycle mid-infrared continuum spanning from 500 to 2250 cm^{-1}," Light. Sci. Appl. **7**(2), 17180–17180 (2017).

[18]U. Elu, L. Maidment, L. Vamos, F. Tani, D. Novoa, M. H. Frosz, V. Badikov, D. Badikov, V. Petrov, P. St. J. Russell, and J. Biegert, "Seven-octave high-brightness and carrier-envelope-phase-stable light source," Nat. Photonics **15**(4), 277–280 (2021).

[19]A. S. Kowligy, A. Lind, D. D. Hickstein, D. R. Carlson, H. Timmers, N. Nader, F. C. Cruz, G. Ycas, S. B. Papp, and S. A. Diddams, "Mid-infrared frequency comb generation via cascaded quadratic nonlinearities in quasi-phase-matched waveguides," Opt. Lett. **43**(8), 1678 (2018).

[20]L. Zhou, X. Qin, Y. Di, H. Lou, J. Zhang, Z. Deng, C. Gu, D. Luo, and W. Li, "Frequency comb with a spectral range of 0.4–5.2 μm based on a compact all-fiber laser and $LiNbO_3$ waveguide," Opt. Lett. **48**(17), 4673 (2023).

[21]J. Neu and C. A. Schmuttenmaer, "Tutorial: An introduction to terahertz time domain spectroscopy (THz-TDS)," J. Appl. Phys. **124**(23), 231101 (2018).

[22]N. M. Burford and M. O. El-Shenawee, "Review of terahertz photoconductive antenna technology," Opt. Eng. **56**(1), 010901 (2017).

[23]K. R. Allakhverdiev, M. Ö. Yetis, S. Özbek, T. K. Baykara, and E. Y. Salaev, "Effective nonlinear GaSe crystal. Optical properties and applications," Laser Phys. **19**(5), 1092–1104 (2009).

[24]M. Hagner, P. Sulzer, A. Liehl, M. Cimander, H. Kempf, A. Bitzer, A. Herter, and A. Leitenstorfer, "Ultrabroadband suppression of mid-infrared reflection losses of a layered semiconductor by nanopatterning with a focused ion beam," Opt. Express **29**(21), 33632 (2021).

[25]Q. Wu and X. C. Zhang, "Free-space electro-optics sampling of mid-infrared pulses," Appl. Phys. Lett. **71**(10), 1285–1286 (1997).

[26]A. Leitenstorfer, S. Hunsche, J. Shah, M. C. Nuss, and W. H. Knox, "Detectors and sources for ultrabroadband electro-optic sampling: Experiment and theory," Appl. Phys. Lett. **74**(11), 1516–1518 (1999).

[27]D. Brida, G. Krauss, A. Sell, and A. Leitenstorfer, "Ultrabroadband Er: Fiber lasers," Laser Photonics Rev. **8**(3), 409–428 (2014).

[28]A. Sell, G. Krauss, R. Scheu, R. Huber, and A. Leitenstorfer, "8-fs pulses from a compact Er:fiber system: quantitative modeling and experimental implementation," Opt. Express **17**(2), 1070–1077 (2009).

[29]A. Budweg, D. Yadav, A. Grupp, A. Leitenstorfer, M. Trushin, F. Pauly, and D. Brida, "Control of excitonic absorption by thickness variation in few-layer GaSe," Phys. Rev. B **100**(4), 045404 (2019).